The International Journal of Advanced Manufacturing Technology (2019) 103:1297–1308
https://doi.org/10.1007/s00170-019-03611-7

ORIGINAL ARTICLE

Joining phenomena and tensile strength of joint between Ni-based superalloy and heat-resistant steel by friction welding

M Kimura[1] · K Nakashima[2] · M Kusaka[1] · K Kaizu[1] · Y Nakatani[3] · M Takahashi[4]

Received: 20 July 2018 / Accepted: 18 March 2019 / Published online: 3 April 2019
© Springer-Verlag London Ltd., part of Springer Nature 2019

Abstract

In order to obtain easily good joint with no crack at the interface between Ni-based superalloy (Ni-SA) and heat-resistant steel (HRS), the investigation of weldability in those material combinations by friction welding method is required. This paper described the joining phenomena and the tensile strength of the friction-welded joint between Ni-SA and HRS. The joining phenomena during the friction process, such as joining behaviour and friction torque, were measured. The effects of friction pressure, friction time, and forge pressure on the joint tensile strength were also investigated, and the characteristics of joints were observed and analysed. The good joint, which had the fracture in the HRS base metal and the tensile strength of its base metal with no crack at the weld interface, could be successfully achieved, although it had the hardened and softened areas at the adjacent region of the weld interface. In conclusion, it was found that the joint should be made with an opportune friction time after the HRS side was transferred to the entire weld interface on the Ni-SA side and with adding high forge pressure such as 360 MPa. Hence, the good joint could be obtained by friction welding method.

Keywords Friction welding · Ni-based superalloy · Heat-resistant steel · Friction welding condition · Joint strength · Fracture

1 Introduction

Ni-based superalloy has some characteristics, such as excellent corrosion resistance and outstanding strength under elevated temperatures. This material is widely used as some important parts in aerospace vehicles, industrial gas turbines, gas and/or oil production platform, and so on [1, 2]. To improve those characteristics in Ni-based superalloy, a various kind of those is produced by adding some elements [3, 4]. Also, NiTi alloy, such as shape memory alloy, can regard as a kind of Ni-based superalloy [5, 6]. However, Ni-based superalloy is generally being known as an expensive material than steel. Hence, it can be considered that Ni-based superalloy should be used with combining other inexpensive material, such as steel from a standpoint of an expansion in the use of this material in industrial field. On the other hand, the adjacent region of the interface of joints with Ni-based superalloy has such some degradation as the coarsening of strengthening precipitates [4] and/or the generating of solidification cracking [7] by the conventional fusion welding processes. In addition, it is considered that the mechanical properties of the fusion-welded joint between Ni-based superalloy and other materials, such as steel, are affected due to the microstructural transformation at the adjacent region of the interface by solidification segregation [8], cracking [9–11], and so on. That is, the similar and/or dissimilar joints with Ni-based superalloy have some problems. To solve those problems, the effect of some content elements in Ni-based superalloy was investigated by some authors [12, 13]. The joint strength with Ni-based superalloy was also improved by heat treatment after welding, which was described by many authors [14–21]. Nevertheless, a welding process for easily making the dissimilar joint between Ni-based superalloy and other material, which will result in less degradation of the mechanical and metallurgical properties of the joint, is urgently required due to a viewpoint of reduction in cost for the manufacturing.

✉ M Kimura
mkimura@eng.u-hyogo.ac.jp

[1] Department of Mechanical Engineering, Graduate School of Engineering, University of Hyogo, 2167 Shosha, Himeji, Hyogo 671-2280, Japan

[2] Graduate student, University of Hyogo, 2167 Shosha, Himeji, Hyogo 671-2280, Japan

[3] Toshiba Energy Systems & Solutions Corporation, 2-4 Suehiro-cho, Tsurumi-ku, Yokohama, Kanagawa 230-0045, Japan

[4] Department of Mechanical Engineering, Faculty of Engineering, Nishinippon Institute of Technology, 1-11 Niitsu, Kanda-machi, Miyako-gun, Fukuoka 800-0394, Japan

The solid state joining methods, such as diffusion welding, friction welding, and friction stir welding, can be applied to join dissimilar materials combinations. Friction welding is especially one of welding methods to overcome the previously mentioned limitations, because it is able to avoid for defects related to melting as well as solidification process in fusion welding. In this connection, for example, Sakane et al. [22] investigated the fatigue strength of friction-welded joint between high Ni steel and low alloy steel. Tasaki et al. [23] studied the tensile strength of friction-welded joint between alloy 713C in Ni-based superalloy and nitriding steel. Uemura et al. [24] described the reaction layer at the weld interface of friction-welded joint between alloy-713C in Ni-based superalloy and bearing steel. Luo et al. [25] proposed the inertia friction welding method with additional electronic current for obtaining high quality joint between Ni-based superalloy and steel. However, an opportune friction welding condition and its guideline for obtaining good joint was not demonstrated. Furthermore, the generating and/or growing the reaction layer, such as the brittle intermetallic compound layer, will occur when the dissimilar metal joints (referred to as dissimilar joints) are operated in elevated temperature environments and/or after post-weld heat treatment [26]. It can be considered that those layers at the joint interface of dissimilar joints will give fatal damage to equipment [27]. In particular, the joint, such as the combination between Ni-based superalloy and some steel such as heat-resistant steel (HRS), will be used under an elevated temperature condition, since HRS has also good mechanical and metallurgical properties into that environment [28–30]. Hence, the friction welding condition for easily obtaining good joint, which has the fracture in the base metal of HRS, primarily needs to be established.

In previous works, some of the authors clarified the joining mechanism of friction-welded joints between various metals and low carbon steel or stainless steel. Then, the good joints with the fracture in the low strength metal side (no fracture at the weld interface) in those above combinations were successfully achieved [31–38], though the friction welding condition differed. If combinations of dissimilar materials between Ni-based superalloy and HRS can be joined using the same method as that shown in previous reports [31–38], the good joint of this combination will be easily obtained.

Based on the above background, the authors have been carrying out research to clarify the joining mechanism during the friction process of dissimilar joint. The authors investigate the joining phenomena during the friction process of friction welds between Ni-based superalloy and HRS in the present work. The authors show the tensile strength of the friction-welded joints under various friction welding conditions, especially the effects of friction time and forge pressure on those. Then, the friction welding condition for good joint, which had the same tensile strength as that of the HRS base metal as well as the fracture in the HRS base metal with no crack at the weld interface, will be suggested. That is, an opportune friction welding condition and its guideline for obtaining good joints will be established.

2 Experimental procedure

The materials used were Ni-based superalloy comparable material of alloy 617 (referred to as Ni-SA) and HRS comparable material of Cr-Mo-V steel (ASTM A470 Grade D Class 8, referred to as HRS) in blocks. The chemical composition of the Ni-SA was 18Cr-9Mo-12.5Co-Al-Ti (wt%), the ultimate tensile strength was 993 MPa, the 0.2% yield strength was 759 MPa, the elongation was 19%, and the Vickers hardness was HV298. The chemical composition of the HRS was 0.3C-1.1Cr-1.3Mo-0.25V (wt%), the ultimate tensile strength was 800 MPa, the 0.2% yield strength was 650 MPa, the elongation was 17%, and the Vickers hardness was HV261, respectively. Two kinds of HRS having similar tensile properties were used for this experiment, although those had slightly different contents, because those blocks were supplied at different times. The difference of results with using those HRS base metals was not confirmed, though those details data were not shown due to space limitations. All materials were used in as-received condition, i.e. those were not processed, such as heat treatment for this experiment. Every block was cut in a rectangular shape and then machined to a 12 mm diameter for the weld faying (contacting) surface as shown in Fig. 1. Also, all specimens had three planes at the diameter of 15 mm part for mounting of itself in the friction welding machine. All weld faying surfaces of specimens were polished by a surface grinding machine before joining to eliminate the effect of surface roughness on the joint mechanical properties [39]. Then, both weld faying surfaces were cleaned by acetone just before welding.

A continuous (direct) drive friction welding machine was used for the joining. HRS specimen was set to the rotating side, and the Ni-SA specimen was set to the fixed side, respectively. In this connection, the opposite setting position of those specimens in the rotating and fixed chucks did not have difference in above position for obtained results. Friction welding condition was set to the following combinations: a friction speed of 27.5 s^{-1} (1650 rpm), friction pressures of 30 or 90 MPa, a range of friction times from 0.04 to 40.0 s, a

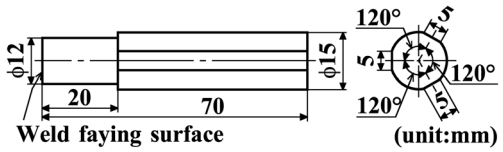

Fig. 1 Shape and dimension of friction welding specimen

range of forge pressures from 30 to 360 MPa, and a forge time of 6.0 s. The authors used three experimental methods as follows.

(1) A conventional friction welding method that has a brake system when the friction time expired. This welding method was carried out for measurement of the friction torque during the friction process.
(2) The welding method that the fixed side specimen is simultaneously and forcibly separated from the rotating side specimen when the friction time expired. This welding method was performed for observation of the transitional changes of the weld interface.
(3) The welding method that the relative speed at the weld interface between both specimens is simultaneously decreased to zero when the friction time expired. To prevent deformation due to braking during rotation stop, this welding method was used. Then, this welding method was performed for investigation of the mechanical and metallurgical properties of joints.

The friction torque was measured with a load cell, and then it was recorded with a personal computer through an A/D converter with a sampling time of 0.001 s. The details of these methods have been also previously described [31–39].

All joint tensile test specimens were machined to 12 mm in the diameter and 66 mm in the parallel length, and those shapes were corresponding to Japanese Industrial Standards [40]. That is, all flash (burr or collar), which was exhausted from the weld interface during the friction welding process, were removed from joints by lathe for joint tensile test specimens. The joint tensile test was performed with as-welded condition at room temperature and was evaluated with joints of the number of three or over per one friction welding condition. To observe the cross-section of joint, the joint was cut at the portion of both sides, which was about 10 mm from the weld interface. Then, it was cut at the longitudinal direction, and the cutting surface was polished for observation of the cross-section of joints. Vickers hardness test at low test force, i.e. the Vickers microhardness (referred to as Vickers hardness), was carried out at room temperature for clarification of the joint properties by using the samples of the cross-section observation. The hardness distribution was measured in the zigzag pattern, and the centre line of it corresponded to the half radius location at the adjacent region of the weld interface. Measuring load was 9.81 N (1 kgf), a measuring range was about 10 mm from the weld interface to both sides, a measuring interval of the longitudinal direction for the joint was 150 μm, and that of the radius direction was 50 μm (amplitude was 100 μm), respectively. SEM observation via EDX analysis was performed to analyse the chemical composition on the adjacent region of the weld interface.

3 Results

3.1 Relationship between joining behaviour and friction torque

At first, the joining phenomena during the friction process were observed. Figure 2 shows the relationship between the joining behaviour and the friction torque curve during the friction process at a friction pressure of 30 MPa. Photos (1) to (6) in Fig. 2a, respectively, correspond to the friction torque of (1) to (6) in Fig. 2b. Photo (1) shows the state of the weld faying surfaces as both surfaces contacted each other, and then, the friction torque was increased. When the friction torque reached the initial peak of (2), the colour of the weld interface was changed with a tinge of red. Immediately after that behaviour, the adjacent region of the weld interface on the HRS side was slightly upset (deformed), and that part was exhausted as flash from the weld interface as shown in Photo (3). The friction torque decreased with increasing friction time and the weld interface was maintained with a colour of whitish-red as shown in Photo (4). Thereafter, the quantities of flash increased with friction time between (4) and (6). The flash was exhausted from the weld interface of the joint during the friction process when the yield stress of the base metal with temperature raise by the friction of both weld faying

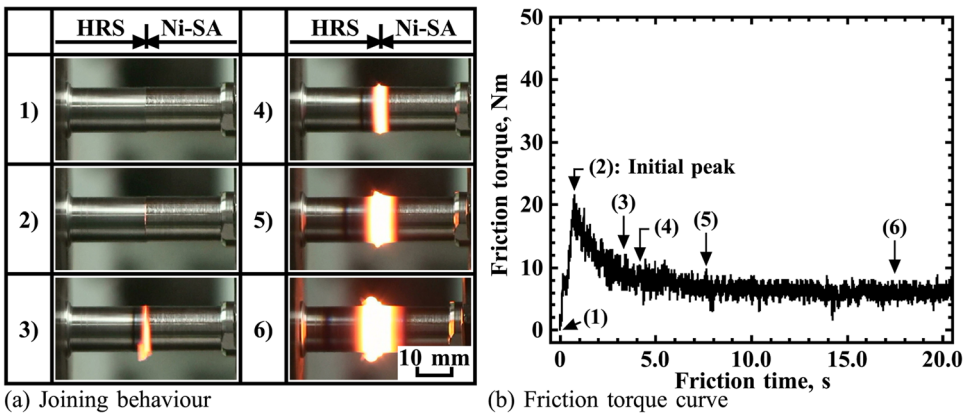

(a) Joining behaviour (b) Friction torque curve

Fig. 2 Joining behaviour and friction torque curve during friction process, which was made with friction pressure of 30 MPa

surfaces was below the applied friction pressure, and it was described in the previous report [41]. Also, the yield strength of HRS base metal was able to estimate lower than that of Ni-SA base metal during the friction process by the considering of the dependence of yield strength on temperature for those base materials [28, 42, 43]. Hence, it could be considered that the flash of HRS was larger than that of Ni-SA (see Fig. 2a). In this connection, if the temperature at the weld interface will be above the melting points of those materials, the flash of the joint will be able to estimate having heavy separation as well as producing the asymmetric shape of that [44, 45]. However, the flash was not separated from the joint during the friction process and the joint had a curl shape flash (demonstrated later) that was similar results in other material combinations of measured temperature [31–38]. Thus, the temperature will be able to be estimated below the melting points of those materials, although further investigation will be naturally needed to elucidate the temperature during the friction process in the material combination in this study. Additionally, the joining behaviour of another friction pressure, such as 90 MPa, resembled those behaviours though the value of the friction torque varied (the friction torque curve with this friction pressure will be demonstrated later).

3.2 Transitional changes of weld interface

Figure 3 shows the examples of the appearances of the weld interfaces after welding at various friction times with a friction pressure of 30 MPa. When a friction time was 0.04 s, i.e. both specimens had been rotated once, the concentric rubbing marks were observed at the peripheral portion of the weld interface of both sides. Also, it was considered that the HRS side transferred to the weld interface on the Ni-SA side, since the area of the concentric rubbing marks on the Ni-SA side was smaller than that of the HRS side and that mark on the Ni-SA side was sparse state. The concentric rubbing marks on the HRS side were extended to the central portions at a friction time of 0.3 s, and the half radius portion of both sides became colourful. Although the concentric rubbing marks increased with friction time, the entire weld interface of both sides did not have that mark when a friction time was 0.7 s, i.e. the friction torque close to the initial peak. When a friction time was 1.5 s, the HRS side had little flashes on the peripheral portion, though the central portion of the Ni-SA side did not have the transferred HRS. When a friction time was 3.0 s, the entire weld interface on the Ni-SA side had the transferred HRS. Thereafter, the quantities of flash of HRS were larger than that of Ni-SA, although those of both sides increased with friction time. Then, both weld interfaces became smooth at a friction time of 20.0 or longer. The transitional changes of the weld interface also resembled those with a friction pressure of 90 MPa, though the quantities of flash differed (data not shown here). This result, which the deformation of HRS side was larger than that of Ni-SA side, was good agreement with the results of joining behaviour (see Fig. 2a).

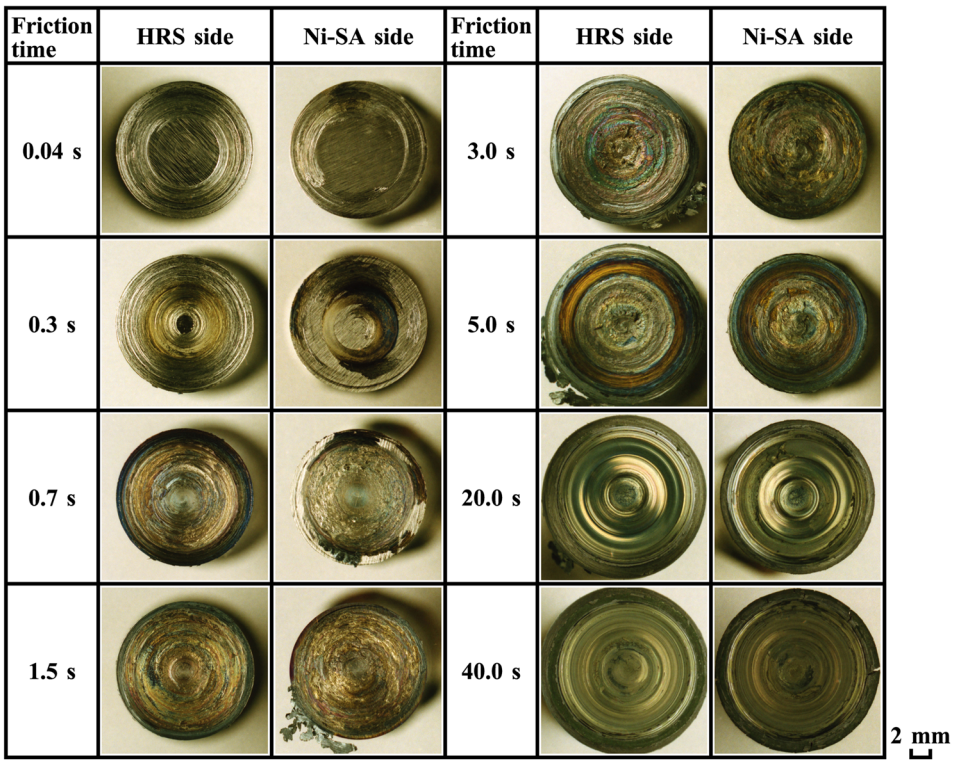

Fig. 3 Appearances of weld interfaces after welding at various friction times, which was made with friction pressure of 30 MPa. **a** Friction pressure of 30 MPa. **b** Friction pressure of 90 MPa

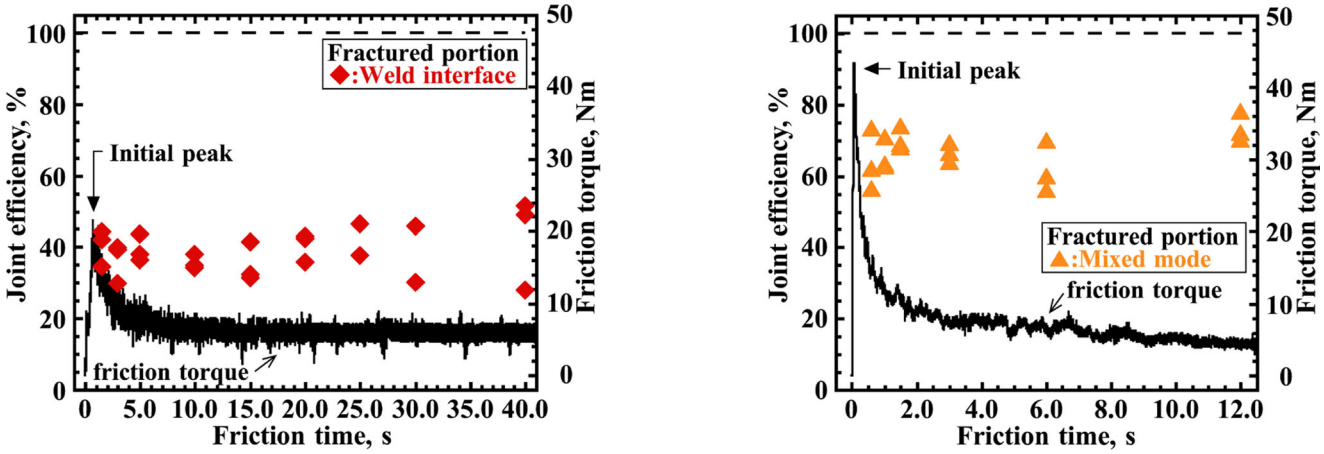

(a) Friction pressure of 30 MPa (b) Friction pressure of 90 MPa

Fig. 4 Relationship between friction time and joint efficiency of joints, in relation to friction torque curves: **a** friction and forge pressures of 30 MPa and **b** friction and forge pressures of 90 MPa

3.3 Relationship between tensile strength of joint and friction time

To clarify the joint strength, the effect of friction time on that was investigated. Figure 4 shows the relationship between the friction time and the joint efficiency of joints, and those were plotted alongside the friction torque curve. The joint efficiency was defined as the ratio of joint tensile strength to the ultimate tensile strength of the HRS base metal. In this instance, the forge pressure was applied at an identical friction pressure, i.e. a friction pressure of 30 MPa was a forge pressure of 30 MPa (Fig. 4a) and that of 90 MPa was 90 MPa (Fig. 4b), respectively. Figures 5 and 6 show the typical appearances of the joint tensile-tested specimens and the typical fractured surfaces of those, respectively. When joints were made with a friction pressure of 30 MPa as shown in Fig. 4a, the joint efficiency at a friction time of 1.5 s was approximately 40%. The joint fractured at the weld interface, although it had a little HRS adhering on the weld interface of the Ni-SA side (referred to as weld interface fracture) as shown in Fig. 5a. The central portion of those surfaces showed like slightly brittle state, and the peripheral portion of those had seizure pattern (Fig. 6a). Thereafter, the joint efficiency was almost maintained around 40%, and the fractured portion was not changed in spite of increasing friction time. When the joint was made with a friction pressure of 90 MPa as shown in Fig. 4b, the joint efficiency at a friction time of 0.6 s was approximately 64%. All joints fractured between the weld interface and the HRS or Ni-SA sides (referred to as mixed mode fracture) as shown in Fig. 5b. The whole fractured surfaces also showed like slightly brittle state (see Fig. 6b). In case of this friction pressure, the joint efficiency was almost maintained around 65% and the fractured portion was not changed in spite of increasing friction time.

Figure 7 shows the examples of the cross-sectional appearances of the weld interface region of joints. In these examples, those joints were made with friction and forge pressures of 30 MPa. When the joint was made with a friction time of 1.5 s, it had the not-joined (non-joined, de-bonding) region at the weld interface (top of arrows in Fig. 7a. The joints with other friction times had also the not-joined region. The joint with a friction pressure of 90 MPa had also this region at the weld interface, though the size of those was smaller than that of 30 MPa. The occurrence of the not-joined region is due to a repeated cycle of joining and separation at the weld interface after the initial peak during the friction process [46]. However, the weld interface of the joint, which was made with the condition of the forge pressure having the same value of the friction pressure, was not joined completely, because the not-joined region generated during the friction process was not able to be reduced during the forge process.

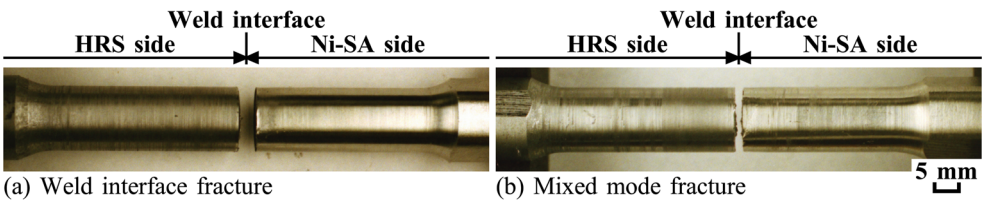

(a) Weld interface fracture (b) Mixed mode fracture

Fig. 5 Typical appearances of joint tensile-tested specimens: **a** weld interface fracture and **b** mixed mode fracture

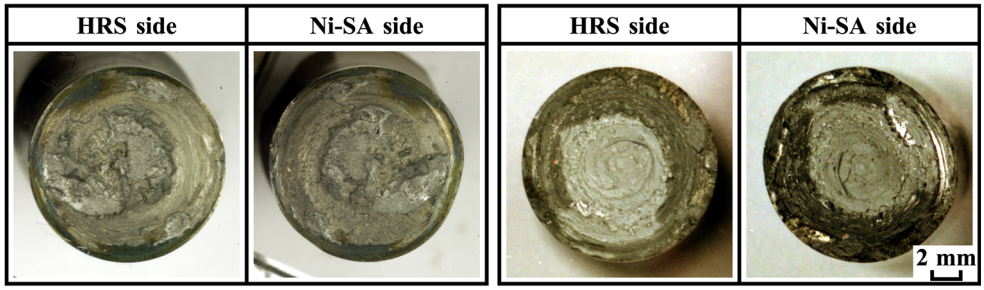

(a) Friction pressure of 30 MPa (b) Friction pressure of 90 MPa

Fig. 6 Typical fractured surfaces of joint tensile-tested specimens: **a** friction and forge pressures of 30 MPa and **b** friction and forge pressures of 90 MPa

3.4 Relationship between tensile strength of joint and forge pressure

To decrease the not-joined region at the weld interface of the joint and to improve the joint efficiency, the effect of forge pressure on joint efficiency was investigated. Figure 8 shows the relationship between the forge pressure and the joint efficiency of joints with a friction pressure of 30 MPa. Figure 9 shows the typical appearances of the joint tensile-tested specimens of joints with adding forge pressure. When joints were made with a friction time of 1.5 s as shown in Fig. 8a, the joint efficiency increased with increasing forge pressure. The fractured portion of joints changed to the mixed mode fracture (Fig. 5b or Fig. 9a) from the weld interface fracture (Fig. 5a). In particular, the joints with a forge pressure of 180 MPa or higher had the local constriction part (necking) at the HRS and/or Ni-SA side (see Fig. 9a). However, the joint efficiency of 100% with the fracture in the HRS base metal was not achieved at a friction time of 1.5 s. Hence, although the not-joined region decreased, it was clarified that the low generating friction heat at this friction time was not able to be welded completely of the entire weld interface as well as the quantity of the transferred HRS on the weld interface at the Ni-SA side was little (Fig. 3). On the other hand, when joints were made with a friction time of 3.0 s as shown in Fig. 8b, the joint efficiency increased with increasing forge pressure, and it had approximately 100% at a forge pressure of 180 MPa. One of the joints with a forge pressure of 270 MPa had the joint efficiency of 100% with the fracture in the HRS base metal (referred to as HRS base metal fracture) as shown in Fig. 9b. Then, all joints with a forge pressure of 360 MPa had the HRS base metal fracture. Those had no crack at the weld interface. The joint efficiency of 100% and the HRS base metal fracture was also achieved when those were made with a friction time of 40.0 s and a forge pressure of 360 MPa (Fig. 8c). If the joint had the not-joined, it will be having the mixed mode fracture since that will be the origin of the fracture. However, the joint with the HRS base metal fracture did not have the not-joined region at the weld interface as shown in Fig. 10. In addition, it could be considered that the adjacent region of the weld interface, which had some weak points due to the contents in both base metals, was exhausted as flash from the weld interface during the forge process.

Figure 11 shows the results of tensile test of joints at various friction welding conditions. Those results were evaluated by the joint tensile test that test was carried out with the number of three or over. In those graphs, the red cross symbols were showed as the results of all joints without the HRS base metal fracture, i.e. that was the weld interface fracture and/or the mixed mode fracture (Fig. 5). The green triangle symbols were showed as the results of joints of which had the weld interface fracture and/or the mixed mode fracture as well as the HRS base metal fracture (Fig. 9b). The blue circular symbols were demonstrated as the results of all joints with the HRS base metal fracture. When joints were made with a friction pressure of 30 MPa as shown in Fig. 11a, all joints with a forge pressure of 90 MPa or below had the weld interface fracture and/or the

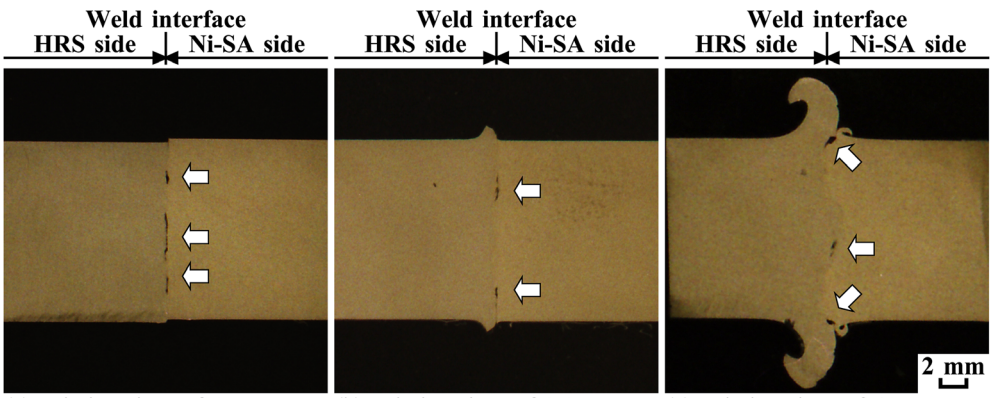

(a) Friction time of 1.5 s (b) Friction time of 3.0 s (c) Friction time of 40.0 s

Fig. 7 Cross-sectional appearances of weld interface regions of joints, which was made with friction and forge pressures of 30 MPa: **a** friction time of 1.5 s, **b** friction time of 3.0 s, and **c** friction time of 40.0 s

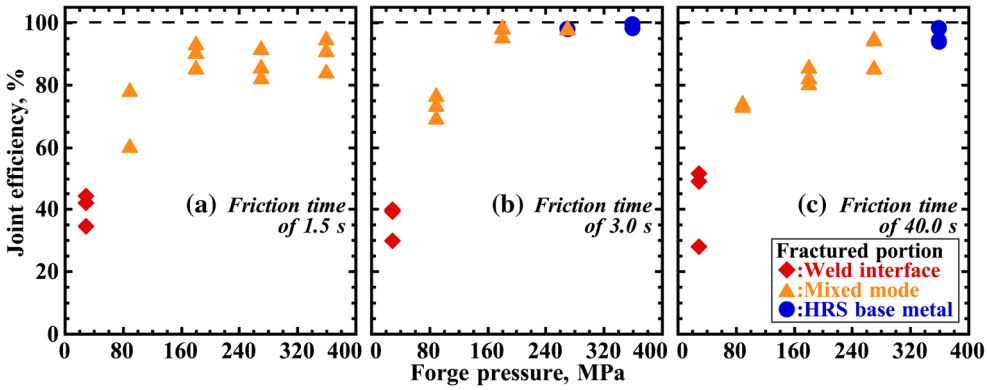

Fig. 8 Relationship between forge pressure and joint efficiency of joints, which was made with friction pressure of 30 MPa at various friction times: **a** friction time of 1.5 s, **b** friction time of 3.0 s, and **c** friction time of 40.0 s

mixed mode fracture. However, all joints with the HRS base metal fracture with reliability were obtained at a friction time of 3.0 s or longer with a forge pressure of 360 MPa. In particular, this friction time of 3.0 s under a friction pressure of 30 MPa corresponded to the time when the entire Ni-SA side had the transferred HRS (see Fig. 3). The HRS base metal fracture with reliability was also obtained at a friction time of 1.0 s or longer with a forge pressure of 360 MPa when joints were made with a friction pressure of 90 MPa as shown in Fig. 11b. When the entire weld interface on the Ni-SA side had the transferred HRS, a friction time of 1.0 s under a friction pressure of 90 MPa also corresponded to that time. Therefore, it was clarified that the friction time should be set to the time after the entire weld interface on the Ni-SA side had the transferred HRS with high forge pressure such as 360 MPa.

3.5 Investigation of characteristics for joint with HRS base metal fracture

Based on the above results, the joint obtaining the HRS base metal fracture with reliability as shown in Fig. 9b was able to make. To clarify the characteristics of the joint in details, the hardness test of those was carried out. Figure 12 shows the examples of Vickers hardness distribution across the weld interface at the half radius location of joints. In these cases, those joints were made with a friction pressure of 30 MPa and a forge pressure of 360 MPa. When the joint was made with a friction time of 3.0 s as shown in Fig. 12a, it had the hardened area that extended about 1.5 mm in the longitudinal direction of the HRS side. This joint also had the softened area in the longitudinal direction and that extended from about 1.5 to 3.0 mm of the HRS side and the extended from the weld interface to 1.5 mm of the Ni-SA side, respectively. The joint with a friction time of 40.0 s had also the hardened and softened areas (Fig. 12b). The softened area of this joint was larger than that of the joint with a friction time of 3.0 s due to large heat input. However, the hardened area of this joint was similar to that of the joint with a friction time of 3.0 s, though it had slightly scattering. Hence, it was able to estimate that cooling speed after welding of those joints were similar in spite of the flash differed. The joints with other friction welding conditions as well as another measuring location of this joint also had those areas. If the joint had high susceptibility of cracking in the hardened area during the welding process [47], it will be not having the HRS base metal fracture since that will be the origin of the fracture. Also, the hardened area seems to be not affected to the joint strength of joint for similar materials combination in this study [10]. Furthermore, the softened region also was not affected to the joint strength of joint because the joint fractured at the portion, which occurred in the HRS side beyond out of that area as shown in Fig. 9b. Therefore, it was clarified that the joint had the joint efficiency of 100% and the HRS base metal fracture by plastic constraint, although those had the hardened and softened areas.

Figure 13 shows the SEM images and EDX analysis results on the adjacent region of the weld interface at the half radius location of the joint. In this case, this joint was made with a friction pressure of 30 MPa, a friction time of 3.0 s, and a forge pressure of 360 MPa. Also, Fig. 13a showed the results of the plane scanning, and Fig. 13b showed the results of the line scanning, respectively. The weld interface was clear as shown in the micrograph photo of Fig. 13a. The remarkable concentration of the Fe, Ni, and Cr was observed at the adjacent region of the weld interface on the HRS side by EDX analysis, and this area had the light colour part of Fe and the dark colour parts of Ni and Cr, i.e. some of a differing concentration part.

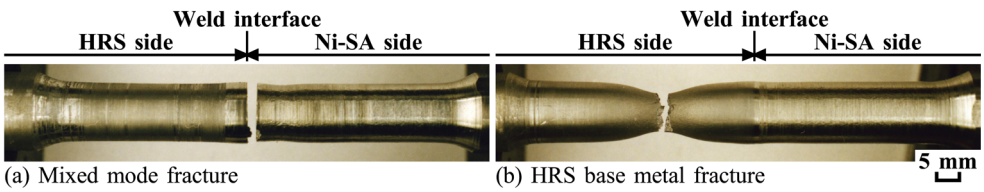

(a) Mixed mode fracture (b) HRS base metal fracture

Fig. 9 Typical appearances of joint tensile-tested specimens with adding forge pressure: **a** mixed mode fracture and **b** HRS base metal fracture

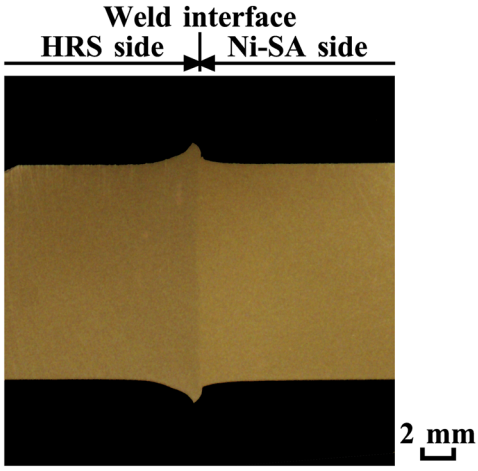

Fig. 10 Cross-sectional appearance of weld interface region of joint, which was made with friction pressure of 30 MPa, friction time of 3.0 s, and forge pressure of 360 MPa. **a** Friction pressure of 30 MPa and **b** Friction pressure of 90 MPa

Furthermore, the distribution lines corresponding to Fe, Ni, and Cr by EDX analysis had a plateau part on the adjacent region of the HRS side, and those lines had large scattering (Fig. 13b). However, the evidence of the intermetallic compound layer at this layer also could not be obtained that included the results of the point scanning of EDX. Therefore, it was considered that the adjacent region of the HRS side had the lamellar structures between HRS and Ni-SA, and it was the mechanically mixed (mechanical mixing) layers. The width (distance from the weld interface in the longitudinal direction of the joint) of that was approximately 150 μm. It was found that the intermetallic compound layer could not be observed with respect to the joint though that might be included of the intermediate interlayer due to the structure change, because it did not have a steady plateau part without scattering of those analysed contents, which was based on SEM observation level. The intermetallic compound layer that influences joint strength was not also observed in the joint with other friction welding conditions as well as another measuring location of this joint, in spite of the width of the mechanically mixed layer differed. That mechanically mixed layer was able to estimate like an austenitic structure in consideration of the other analysed results as well as the joint had the hardened area (Fig. 13). A similar mechanically mixed layer was also observed even in several friction-welded joints for dissimilar materials combination as reported by many researchers [39, 48–54]. The mechanically mixed layer seems to be a cause of the influence of the joint strength of some dissimilar friction-welded joints [39, 53, 54]. Furthermore, some of fusion-welded joint of the similar material combination in this study did not have good tensile strength due to the producing of the intermetallic compound layer at the weld interface [55, 56]. Nevertheless, the mechanically mixed layer of the joint in this study was not affected to the joint strength, since this joint had the joint efficiency of 100% with the HRS base metal fracture (see Fig. 9b). Naturally, it could be considered that the dissolution of precipitates [57, 58] as well as the structure change [13, 18, 29] at the adjacent region of the weld interface of the joint will occur during the friction process, because the highest temperature portion was the weld interface. However, it was able to be considered that the most of that structure as well as high temperature area were exhausted as flash by adding high forge pressure, since the joint with the HRS base metal fracture was obtained by that pressure condition (360 MPa). Furthermore, it was able to consider that the mechanically mixed layer was generated due to the heavy plastic flow of both base metals during the friction process, because both materials were not formed as the lamellar structures if the temperature at the weld interface had above the melting point during the friction process. In this consideration, those clarifications will be a future investigation subject and further investigation will be needed to elucidate the detailed characteristics of that layer by other analysis system, such as TEM and XRD

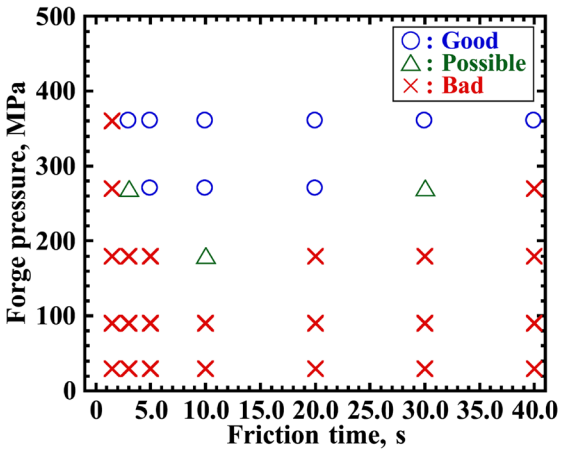

(a) Friction pressure of 30 MPa

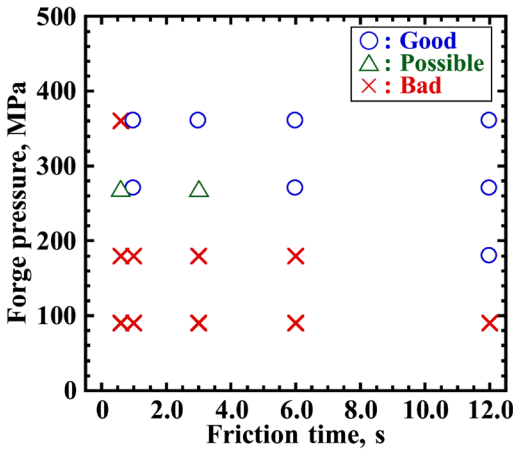

(b) Friction pressure of 90 MPa

Fig. 11 Results of tensile test of joints at various friction welding conditions: **a** friction pressure of 30 MPa and **b** friction pressure of 90 MPa. **a** Friction time of 3.0 s and **b** friction time of 40.0 s

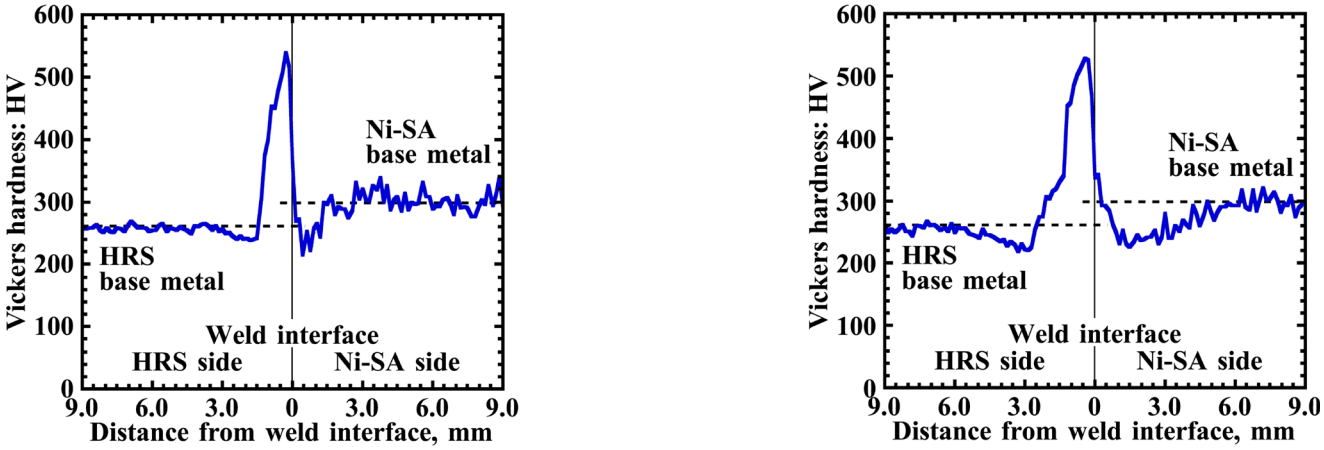

(a) Friction time of 3.0 s (b) Friction time of 40.0 s

Fig. 12 Vickers hardness distributions across weld interface at half radius location of joints which was made with friction pressure of 30 MPa and forge pressure of 360 MPa: **a** friction time of 3.0 s and **b** friction time of 40.0 s. **a** Plane scanning result. **b** Line scanning result

analyses for the dissimilar joint as well as making mechanism of this layer.

4 Discussion

According to the result described above, the friction welding conditions for obtaining good joints, of which had the joint efficiency of 100% with the HRS base metal fracture, were demonstrated. To estimate the opportune friction time, the joint appearances were observed. Figure 14 shows the examples of appearances of joints at various friction times. In these examples, those were made with a friction pressure of 30 MPa and a forge pressure of 360 MPa and those joints fractured in the HRS base metal (Fig. 9b). The quantities of flashes of both sides increased with friction time, and the flash of the HRS side was larger than that of the Ni-SA side. Ni-based superalloy is generally known as an expensive material than steel, of

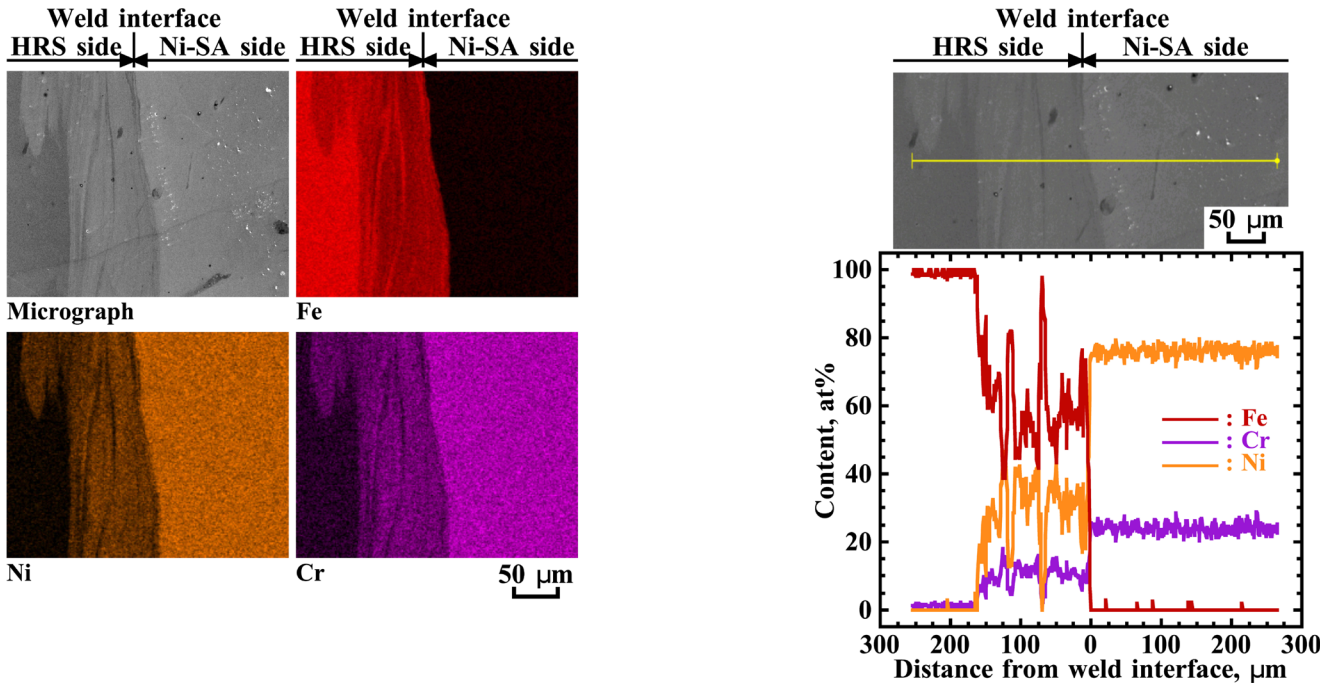

(a) Plane scanning result (b) Line scanning result

Fig. 13 SEM images and EDX analysis results at adjacent region of weld interface at half radius location for joint, which was made with friction pressure of 30 MPa, friction time of 3.0 s, and forge pressure of 360 MPa

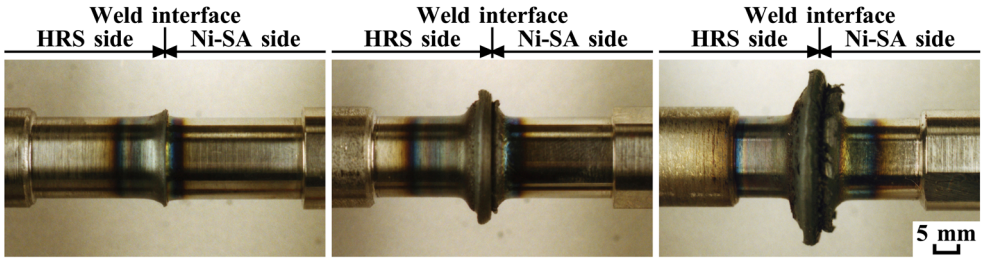

(a) Friction time of 3.0 s (b) Friction time of 10.0 s (c) Friction time of 40.0 s

Fig. 14 Appearances of joints, which was made with friction pressure of 30 MPa and forge pressure of 360 MPa at various friction times: **a** friction time of 3.0 s, **b** friction time of 10.0 s, and **c** friction time of 40.0 s

which was described in the introduction section. In particular, from a viewpoint of reduction of a manufacturing cost, it is desirable to be able to decrease flash of the Ni-SA side from the joint. In addition, the axial shortening (burn-off) of the joint with correspond to Fig. 14 at a friction time of 3.0 s was about 0.9 mm, that of 10.0 s was about 5.0 mm, and that of 40.0 s was about 13.6 mm, respectively. That is, the flash quantity and the axial shortening of the joint with a friction time of 3.0 s were smaller than those of 40.0 s. Furthermore, the softened region of the joint with a friction time of 3.0 s was smaller than that of 40.0 s (see Fig. 12). Additionally, the weld interface is not held to high temperature condition, such as Figs. 2a–6) when the joint will be made with short friction time. Hence, it is able to suggest that the friction time should be set to the time when the entire weld interface on the Ni-SA side had the transferred HRS. Thus, a guideline of an opportune friction welding condition for obtaining good joints was established. Further investigation must elucidate the detailed characteristics of the joint as the fatigue and creep strengths as well as the tensile strength under high temperature conditions, since some researchers proposed the improvement of the joint strength of some Ni-based superalloy and dissimilar metal combination [14, 15], HRS and dissimilar metal combination [29], and the same metal combination [16–19, 21] by post-weld heat treatment. Those topics are also a future investigation subject. However, the joint should be made with an opportune friction time after the HRS side was transferred to the entire Ni-SA side and with high forge pressure, such as 360 MPa.

5 Conclusions

This study described the joining phenomena and tensile strength of the friction-welded joint between Ni-based superalloy (Ni-SA) and HRS. The following conclusions are provided.

(1) The joining was welded with the HRS transferred to the weld interface on the Ni-SA side. The flash of HRS was larger than that of Ni-SA, although those of both sides increased with friction time. In addition, the joining phenomena during the friction process at a friction pressure of 30 MPa resembled those of 90 MPa.

(2) The joint, which was made with a forge pressure of an identical friction pressure, did not have the joint efficiency of 100% in spite of friction time. Those joints had the not-joined region at the weld interface.

(3) All joints with the joint efficiency of 100% and the HRS base metal fracture with reliability were obtained at a friction time of 3.0 s or longer with a forge pressure of 360 MPa. Also, the HRS base metal fracture with reliability was also obtained at a friction time of 1.0 s or longer with a forge pressure of 360 MPa when joints were made with a friction pressure of 90 MPa. Those joints had no crack at the weld interface after the tensile testing.

(4) The joints with the joint efficiency of 100% and the HRS base metal fracture had both the hardened and softened areas at the adjacent region of the weld interface on those. The hardened and softened areas increased with friction time.

In conclusion, the joint should be made with an opportune friction time after the HRS side was transferred to the entire weld interface on the Ni-SA side and with adding high forge pressure, such as 360 MPa.

Acknowledgements The authors wish to thank the staff members of the Machine and Workshop Engineering at the Graduate School of Engineering, University of Hyogo. Also, we wish to thank Mr. Shigekazu Miyashita in Toshiba Corporation Energy Systems & Solutions Company for his kindly and aggressive assisting to this study.

References

1. American Welding Society (1996) Welding hand book, vol 3, 8th edn. American Welding Society, Miami, FL, pp 218–288
2. Oinuma S, Nakatani Y, Imai K, Takahashi T, Sasaki T (2018) Effect of stress and atmosphere on grain boundary oxidation of Ni-based superalloy for 700 °C A-USC steam turbine. Trans JSME 84(859): Doc. No. 17-00383 (in Japanese)
3. Yoshinari A (2001) Application and properties of Ni-based superalloy castings. J Jpn Foundrymen's Soc 73(12):834–839 (in Japanese)
4. Sugahara K (2015) Guidelines for the selection of corrosion-resistant non-ferrous metals IV: nickel- based alloy. J Soc Mater Sci, Jpn 64(1):57–62 (in Japanese)
5. Oliveira JP, Miranda RM, Braz Fernandes FM (2017) Welding and joining of NiTi shape memory alloys: a review. Prog Mater Sci 88: 412–466
6. Li Q, Zhu Y (2018) Impact butt welding of NiTi and stainless steel—an examination of impact speed effect. J Mater Process Technol 255:434–442

7. Ebrahimnia M, Ghaini FM, Shahverdi HR (2014) Hot cracking in pulsed laser processing of a nickel based superalloy built up by electrospark deposition. Sci Technol Weld Join 19(1):25–29
8. Inoue H, Honma R, Fukumoto S (2012) Effect of dilution on microstructures of dissimilar weld metals using nickel base alloy filler wire—study on microstructures of super austenitic stainless steel weld metals. Q J Jpn Weld Soc 30(1):9–18 (in Japanese)
9. Ikawa H (1968) Precipitated phase and weld crackings of Ni-Base superalloy. J Jpn Weld Soc 38(9):979–990 (in Japanese)
10. Oiwa M, Kumai S (2011) Microstructure and tensile strength of electron-beam-welded nickel base-superalloy/alloy steel dissimilar joints. Q J Jpn Weld Soc 29(1):35–40 (in Japanese)
11. Saida K, Bunda K, Ogiwara H, Nishimoto K (2013) Microcracking susceptibility in dissimilar multipass welds of Ni-base alloy 690 and low-alloy steel. Q J Jpn Weld Soc 31(3):181–192 in Japanese
12. Ohsasa K, Nakaue S, Kudoh M, Narita T (1995) Analysis of solidification path of Fe-Cr-Ni ternary alloy. ISIJ Int 35(6):629–636
13. Yuan SN, Jia LN, Ma LM, Jiang H, Zhang H (2014) Microstructure and room temperature mechanical properties of hypereutectic Nb-Si based alloy processed by directional solidification. Mater Sci Technol 30(1):75–80
14. Kim J, Kim SH, Choi KJ, Kim JH, Bahn CB, Hwang IS (2014) In-situ investigation of thermal aging effect on oxide formation in Ni-base alloy/low alloy steel dissimilar metal weld interfaces. Corros Sci 86:295–303
15. Daus F, Li HY, Baxter G, Bray S, Bowen P (2007) Mechanical and microstructual assessments of RR1000 to IN718 inertia welds—effects of welding parameters. Mater Sci Technol 23(12):1424–1432
16. Wang H, Ikeuchi K, Aritoshi M, Takahashi M, Ikeda K (2008) Joint strength of friction-welded Inconel 718 alloy and its improvement by post weld heat treatment—joint performance and its controlling factors in friction welding of Inconel 718 alloy. J Jpn Weld Soc 26(2):167–173 (in Japanese)
17. Lalam SV, Reddy GM, Mohandas T, Kamaraj M, Murty BS (2009) Continuous drive friction welding of Inconel 718 and EN24 dissimilar metal combination. Mater Sci Technol 25(7):851–861
18. Andersson J, Sjöberg GP (2012) Repair welding of wrought superalloys: alloy 718, Allvac 718 Plus and Waspaloy. Sci Technol Weld Join 17(1):49–59
19. Ishii K, Kakehi K, Yonemoto T (2012) Effect of TIG welding on microstructure and mechanical properties of Inconel 718. J Jpn Inst Metals 76(5):289–294 (in Japanese)
20. Pouranvari M, Ekrami A, Kokabi AH (2014) Diffusion brazing of cast INCONEL 718 superalloy utilising standard heat treatment cycle. Mater Sci Technol 30(1):109–115
21. Damodaram R, Raman SGS, Rao KP (2014) Effect of post-weld heat treatments on microstructure and mechanical properties of friction welded alloy 718 joints. Mater Des 53:954–961
22. Sakane M, Ohnami M, Wakai T (1992) High temperature low cycle fatigue of high nickel steel-SUH35 friction welded specimens. J Soc Mater Sci, Jpn 41(471):1786–1792 (in Japanese)
23. Tasaki Y, Nakayama N (1970) Friction welding of Ni-based super alloy and nitriding steel. J Jpn Soc Prec Eng 36(11):707–711 (in Japanese)
24. Uemura M, Okita K, Aritoshi M, Seo N, Wakana Y (1995) Friction welding of Inconel 713C to bearing steel. J Jpn Friction Weld Assoc 2(4):203–209 (in Japanese)
25. Luo J, Li L, Dong Y, Xu X (2014) A new current hybrid inertia friction welding for nickel-based superalloy K418-alloy steel 42CrMo dissimilar metals. Int J Adv Manuf Technol 70(9–12):1673–1681
26. Kimura M, Fuji A, Shibata S (2015) Joint properties of friction welded joint between pure magnesium and pure aluminium with post-weld heat treatment. Mater Des 85:169–179
27. American Welding Society (1982) Welding hand book, vol 4, 7th edn. American Welding Society, Miami, FL, pp 537–538
28. Fukui S, Yamada S, Tada K (1981) Effect of Ni on some properties of Cr-Mo-V rotor steel. Electr Furn Steel 52(2):99–106 (in Japanese)
29. Yamazaki M, Watanabe T, Hongo H, Tabuchi M (2008) Creep rupture properties of welded joints of heat resistant steel. J Power Energy Syst 2(4):1140–1149
30. Abe F (2015) Research and development of heat- resistant materials for advanced USC power plants with steam temperature of 700 °C and above. Eng 1(2):211–224
31. Kimura M, Ishii H, Kusaka M, Kaizu K, Fuji A (2009) Joining phenomena and joint strength of friction welded joint between pure aluminium and low carbon steel. Sci Technol Weld Join 14(5):388–395
32. Kimura M, Ishii H, Kusaka M, Kaizu K, Fuji A (2009) Joining phenomena and joint strength of friction welded joint between aluminium-magnesium alloy (AA5052) and low carbon steel. Sci Technol Weld Join 14(7):655–661
33. Kimura M, Suzuki K, Kusaka M, Kaizu K (2017) Effect of friction welding condition on joining phenomena, tensile strength, and bend ductility of friction welded joint between pure aluminium and AISI 304 stainless steel. J Manuf Process 25:116–125
34. Kimura M, Suzuki K, Kusaka M, Kaizu K (2017) Effect of friction welding condition on joining phenomena and mechanical properties of friction welded joint between 6063 aluminium alloy and AISI 304 stainless steel. J Manuf Process 26:178–187
35. Kimura M, Kusaka M, Kaizu K, Fuji A (2009) Effect of friction welding condition on joining phenomena and tensile strength of friction welded joint between pure copper and low carbon steel. J Solid Mech Mater Eng 3(2):187–198
36. Kimura M, Kasuya K, Kusaka M, Kaizu K, Fuji A (2009) Effect of friction welding condition on joining phenomena and joint strength of friction welded joint between brass and low carbon steel. Sci Technol Weld Join 14(5):404–412
37. Kimura M, Iijima T, Kusaka M, Kaizu K, Fuji A (2014) Joining phenomena and tensile strength of friction welded joint between pure titanium and low carbon steel. Mater Des 55:152–164
38. Kimura M, Iijima T, Kusaka M, Kaizu K, Fuji A (2016) Joining phenomena and tensile strength of friction welded joint between Ti-6Al-4V titanium alloy and low carbon steel. J Manuf Process 24(1):203–211
39. Kimura M, Saitoh Y, Kusaka M, Kaizu K, Fuji A (2011) Effect of friction welding condition and weld faying surface properties on tensile strength of friction welded joint between pure titanium and pure copper. J Solid Mech Mater Eng 5(12):849–865
40. Committee JIS (2011) JIS Z 2241 metallic materials—tensile testing—method of test at room temperature. Japanese Industrial Standards. Japanese Industrial Standards Committee, Tokyo (in Japanese)
41. Kimura M, Kusaka M, Seo K, Fuji A (2003) Relationship between joining phenomena and yield strength of substrates of dissimilar friction welding. Q J Jpn Weld Soc 21(3):481–488 (in Japanese)
42. Bennett C (2015) Finite element modelling of the inertia friction welding of a CrMoV alloy steel including the effects of solid-state phase transformations. J Manuf Process 18:84–91
43. Klewer J (2017) 16-Alloy 617 and derivatives. In: Materials for ultra-supercritical and advanced ultra-supercritical power plants. Woodhead Publishing, Cambridge, pp 547–570
44. Jayabharath K, Ashfaq M, Venugopal P, Achar DRG (2007) Investigations on the continuous drive friction welding of sintered powder metallurgical (P/M) steel and wrought copper parts. Mater Sci Eng A 454-455:114–123
45. Kimura M, Shirakami K, Kusaka M, Kaizu K (2014) Joining phenomena and tensile strength of ABS resin friction welded joint. Trans JSME 80(815):SMM0190 No. 14-00175 (in Japanese)
46. Hasui A, Fukushima S (1975) On the torque in friction welding. J Jpn Weld Soc 44(12):1005–1010 (in Japanese)

47. Dehmolaei R, Shamanian M, Kermanpur A (2007) Improving weldability of aged 25Cr-35Ni heat resistant steel/alloy 800 dissimilar welds. Sci Technol Weld Join 12(7):586–592
48. Aritoshi M, Okita K, Enjo T, Ikeuchi K, Matsuda F (1991) Friction welding of oxygen free copper to pure aluminum. Q J Jpn Weld Soc 9(4):467–474 in Japanese
49. Yilmaz M, Kaluc E, Tülbentci K, Karagöz S (1996) Investigation into the weld zone of friction welded C45/HS6-5-2 dissimilar steel joints. J Mater Sci Lett 15(4):360–362
50. Straffelini G, Pellizzari M, Bernardi N (2004) Microstructure and impact behaviour of ASTM A105/AISI 304L friction weldments. Mater Sci Technol 20(5):634–640
51. Meshram SD, Mohandas T, Reddy GM (2007) Friction welding of dissimilar pure metals. J Mater Process Technol 184:330–337
52. Arivazhagan N, Singh S, Prakash S, Reddy GM (2008) An assessment of hardness, impact strength, and hot corrosion behaviour of friction-welded dissimilar weldments between AISI 4140 and AISI 304. Int J Adv Manuf Technol 39(7–8):679–689
53. Kimura M, Inui Y, Kusaka M, Kaizu K, Fuji A (2015) Joining phenomena and tensile strength of friction welded joint between pure aluminum and pure copper. Mech Eng J 2(1):14–00328
54. Ruge J, Thomas K, Eckel C, Sundaresan S (1986) Joining of copper to titanium by friction welding. Weld J 65(8):28–31
55. Li G, Huang J, Wu Y (2014) An investigation on microstructure and properties of dissimilar welded Inconel 625 and SUS304 using high-power Co_2 laser. Int J Adv Manuf Technol 76(5–8):1203–1214
56. Ramkumar KD, Dev S, Saxena V, Choudhary A, Arivazhagan N, Narayanan S (2015) Effect of flux addition on the microstructure and tensile strength of dissimilar weldments involving Inconel 718 and AISI 416. Mater Des 87:663–674
57. Ye X, Hua X, Wu Y, Lou S (2015) Precipitates in coarse-grained heat-affected zone of Ni-based 718 superalloy produced by tungsten inert gas welding. J Mater Process Technol 217:13–20
58. Xu Q, Cao T, Ye F, Xu F, Li H, Fang X, Zhao J (2018) Creep-induced microstructural evolution in a nickel-based superalloy designed for advanced ultra- supercritical boilers. Mater Charact 139: 311–318

Publisher's note Springer Nature remains neutral with regard to jurisdictional claims in published maps and institutional affiliations.